Petroleum Research xxx (xxxx) xxx

Contents lists available at ScienceDirect

Petroleum Research

journal homepage: http://www.keaipublishing.com/en/journals/petroleum-research/

Application of AVO attributes for gas channels identification, West offshore Nile Delta, Egypt

Amir Ismail [a, b, *], Hatem Farouk Ewida [c, 1], Mohammad Galal Al-Ibiary [b, 1], Aldo Zollo [a, 1]

[a] Department of Physics "E. Pancini", University of Naples 'Federico II', Italy
[b] Department of Geology, Faculty of Science, Helwan University, Cairo, Egypt
[c] Exploration General Manager, PERENCO North Sinai Petroleum Company, Cairo, Egypt

ARTICLE INFO

Article history:
Received 18 September 2019
Received in revised form
12 January 2020
Accepted 14 January 2020
Available online xxx

Keywords:
AVO attributes
Offshore Nile Delta
Gas channels
Gas bearing sand zones
AVO crossplots

ABSTRACT

The offshore part of the Nile Delta is considered one of the most prolific provinces for gas production and for future petroleum exploration. Amplitude Variation with Offset (AVO) analysis supported by composite logs considered as one of the best-advanced techniques enables the interpreter to understand the seismic data. It is used to generate a new view of the output results, especially for the identification of gas zones as gas channels by using pre-stack AVO attributes that based on the intercept product gradient (A*B) and the Scaled Poisson's Ratio Change. Free gas, regardless of the percentage show obvious AVO anomaly. Well log data, including gamma-ray, resistivity, and Vp sonic logs are used in the seismic data to well tie and in the generation of the synthetic seismogram. Seismic data conditioning processes with check-shot correction is performed to improve the resolution of the reflection events and signal to noise ratio. AVO attributes technique, as a direct hydrocarbon indicator, including AVO gradient analysis and AVO crossplot separate the gas levels in the sand-shale sequences. The identified gas-bearing zones consistent with well log data responses. As the main conclusion, we show the visual evidence for the gas-bearing zones by interpreting different AVO responses due to the changes in fluid and rock types.

1. Introduction

The area of study is one of the most promising areas for gas and oil exploration and production (Fig. 1). 58 trillion cubic feet (Tcf) of gas reserves (Nini et al., 2010) have been discovered until now in the Nile Delta province, from several stratigraphic levels, starting from the Oligocene to the Plio-Pleistocene, it is consequently the greatest prolific region for gas production in Egypt. The hydrocarbon potential of the Nile Delta believed to be limited to the Neogene-Quaternary sequence (EGPC, 1994; Abdel Halim, 2001). The Neogene-Quaternary sequence is separated to the main three sedimentary successions: Miocene, Pliocene, and Holocene (Kamel et al., 1998). The Scarab reservoir is one of several NNW-SSE tending submarine channels complexes within the Late Pliocene, El Wastani Formation. These large-scale channels cuts have acted as conduits through which Pliocene sediments were transported from the Paleo-Nile River into the deep-water Mediterranean Basin. Source rocks are formed in the late Mesozoic to early Miocene sediments (Vandré et al., 2007) with Upper Cretaceous black shales containing good quality source rocks with high total organic content. Fig. 2 shows the stratigraphic column of the Nile Delta.

The Scarab reservoir is a NNW-SSE trending, Y-shaped channel system that is approximately 16 km long marked with yellow color in Fig. 1. The field is grouped into two main channels, named Channel 1 and Channel 2 respectively. Five development wells are producing from Channel 1 and Channel 2 (Ismail et al., 2019). The two main stacked channels are trending in different directions but intersect and share similar depositional environments. Channel 2 is the oldest and it trends SSE-NNW while Channel 1 is the youngest and it trends more SE-NW, with a later SW-NE-trending channel system developing due to fault reactivation. Channels 1 and 2 are connected where they cross paths. The WDDM concession (Fig. 1) was acquired by BG Group and partners Edison Gas in 1995.

Muskat and Meres (1940) pointed out that there is a strong relationship between the incidence angle and the primary wave reflections by considering a constant value for Poisson's ratio.

* Corresponding author. Department of Physics "E. Pancini", University of Naples 'Federico II', Italy.
E-mail address: amir_ismail@science.helwan.edu.eg (A. Ismail).
[1] Co-authors:Dr. Hatem Farouk Ewida, Prof. Mohammad Galal Al-Ibiary, Prof. Aldo Zollo.

https://doi.org/10.1016/j.ptlrs.2020.01.003

Please cite this article as: Ismail, A et al., Application of AVO attributes for gas channels identification, West offshore Nile Delta, Egypt, Petroleum Research, https://doi.org/10.1016/j.ptlrs.2020.01.003

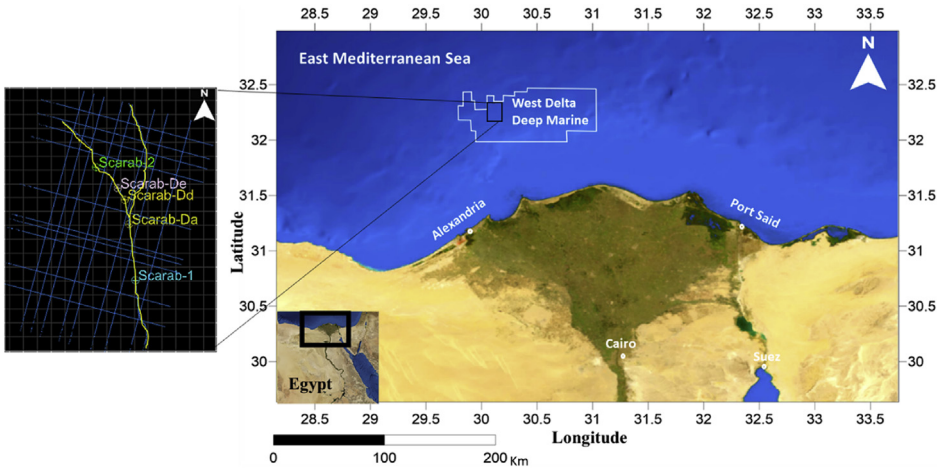

Fig. 1. West Delta Deep Marine concession with the locations of five wells and the 2D-seismic lines, modified from Google Earth.

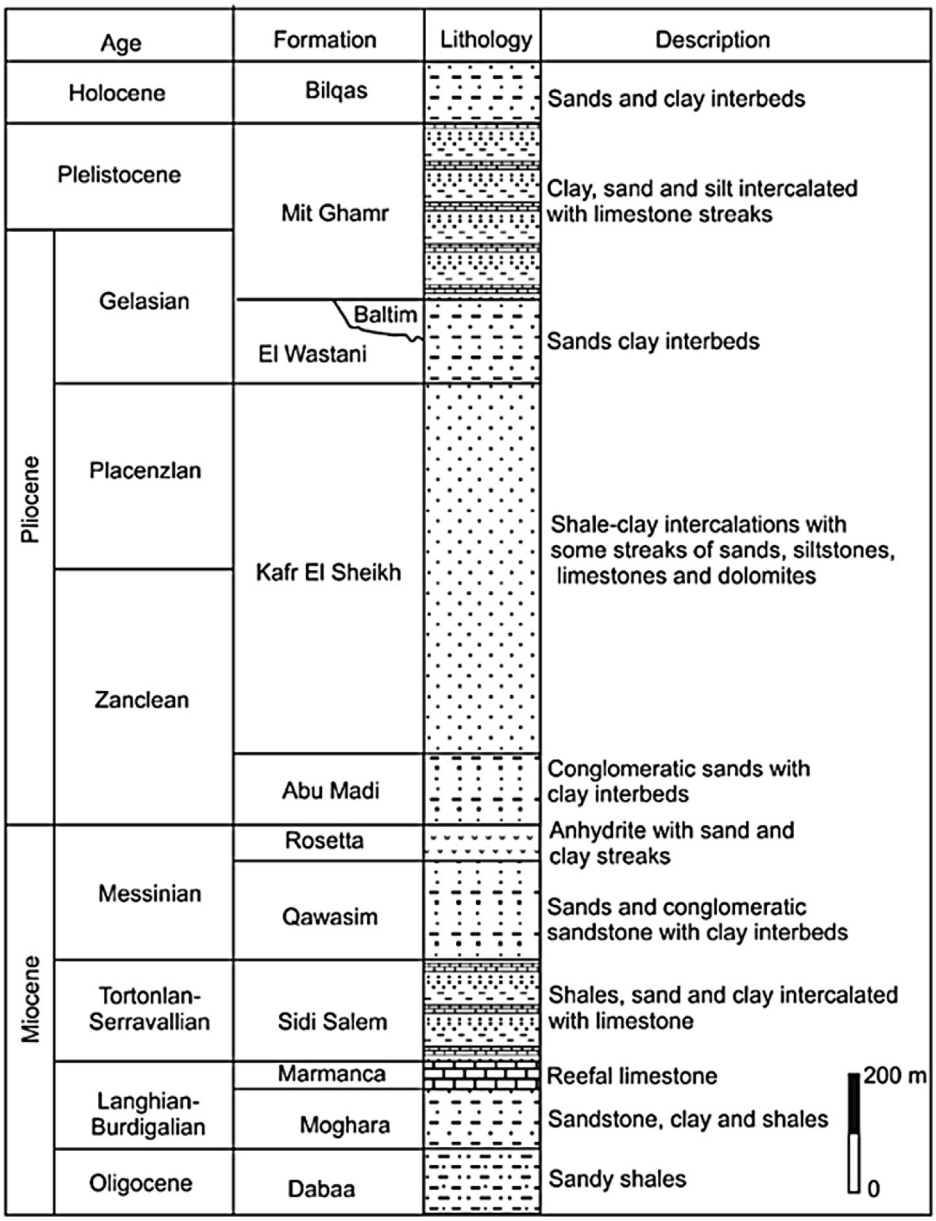

Fig. 2. Nile delta stratigraphic column (Younis et al., 2015).

Please cite this article as: Ismail, A et al., Application of AVO attributes for gas channels identification, West offshore Nile Delta, Egypt, Petroleum Research, https://doi.org/10.1016/j.ptlrs.2020.01.003

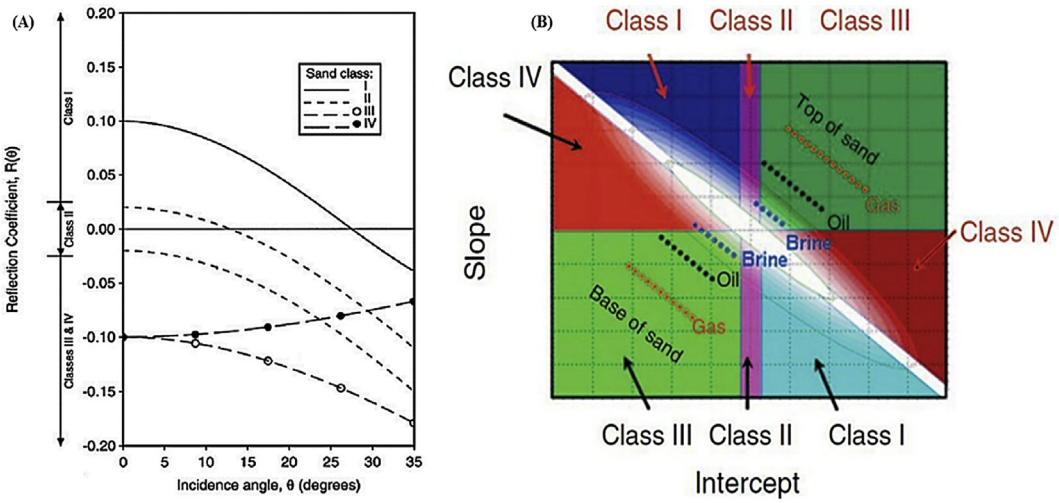

Fig. 3. (A) AVO response curves related to a gas saturated clastic reservoir with shale caprock; in this figure, reflection coefficients changes versus incidence angle are observed in four AVO classes. Class I has a positive normal reflection coefficient and a negative gradient, class II has a small normal reflection coefficient near zero and class III has a negative normal reflection coefficient and a negative gradient (Rutherford and Williams, 1989). Class IV includes a negative normal reflection coefficient but a positive gradient, hence amplitude decreases with increasing offset (Castagna et al., 1998). (B) AVO classification scheme for identifying the magnitude and class of a seismic reflection. The polarity convention in this display denotes a decrease in acoustic impedance by a peak (Foster et al., 2010).

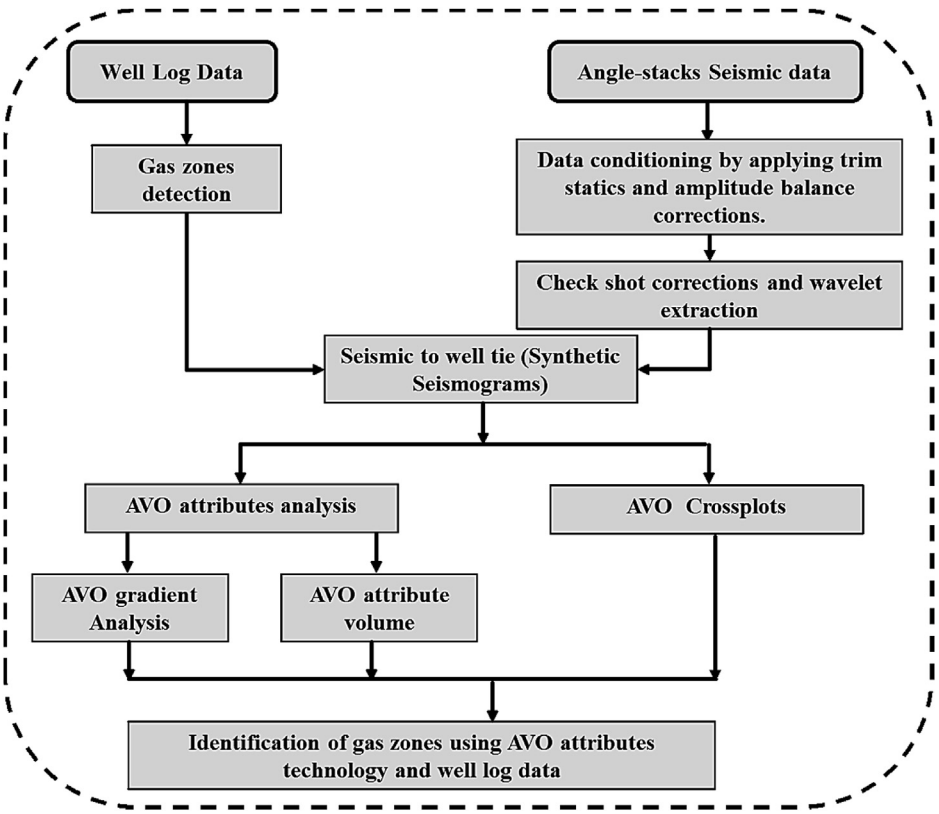

Fig. 4. AVO analysis workflow.

Domenico (1977) pointed out that Poisson's ratio is significantly affected by pore fluid. Aki and Richards' (1980) originate most of the AVO seismic attributes to recognize the hydrocarbon effect by the acoustic impedance and Poisson's ratio. AVO common attributes represented by the intercept (A); the reflection-coefficient gradient (B); P-wave normal-incidence reflectivity, which is equivalent to intercept A; and S-wave normal-incidence reflectivity. From the simplification of Aki and Richards' approximation, Ostrander (1984) described how the AVO analysis can be used to define seismic amplitudes due to gas sands from bright spots caused by non-hydrocarbon-bearing rocks such as igneous rocks (basalts). Rutherford and Williams (1989) depicted different seismic AVO anomalies of gas sands with the same or higher acoustic impedance than the surrounding shale. They presented

Please cite this article as: Ismail, A et al., Application of AVO attributes for gas channels identification, West offshore Nile Delta, Egypt, Petroleum Research, https://doi.org/10.1016/j.ptlrs.2020.01.003

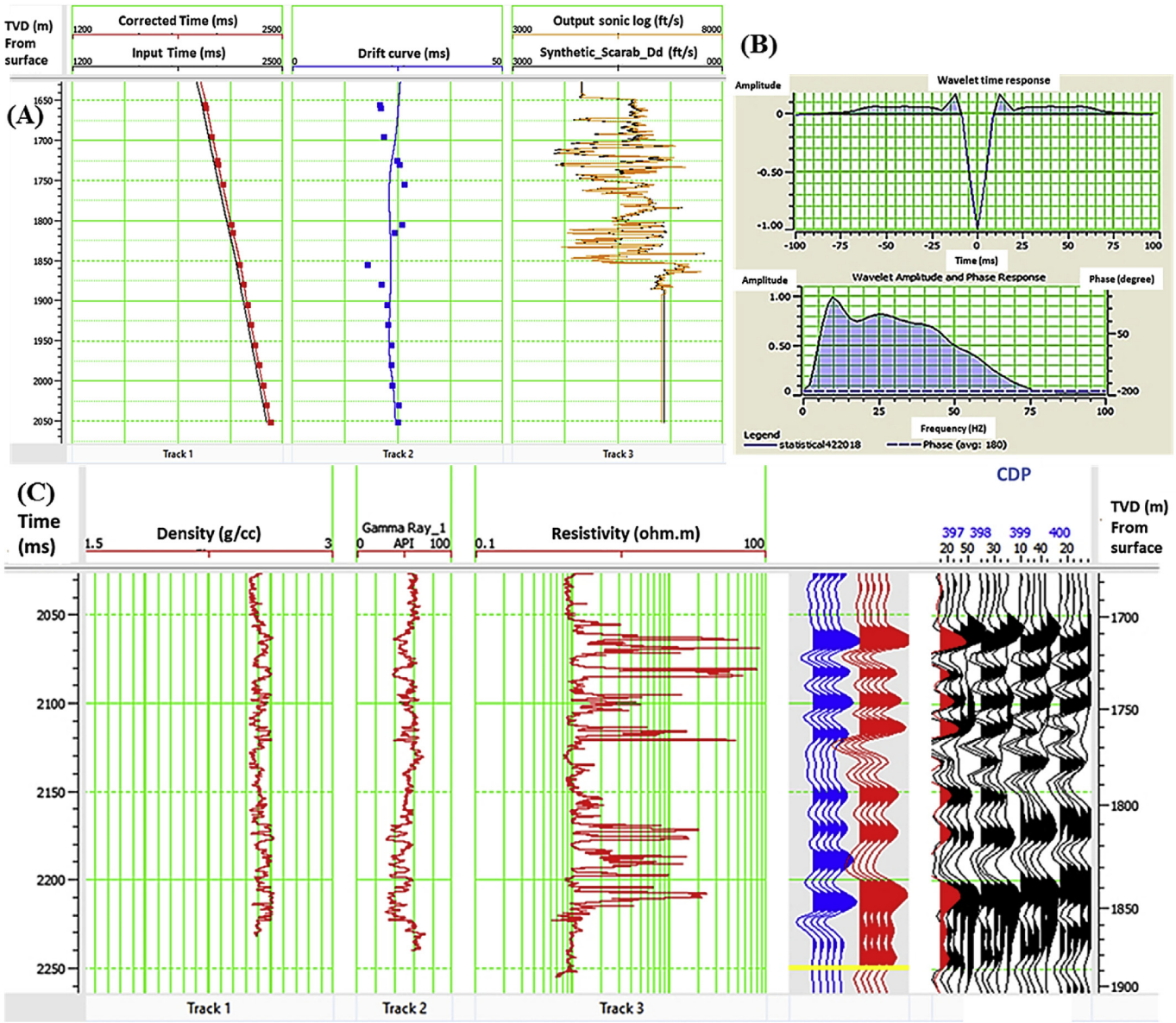

Fig. 5. (A) An example of the check-shot correction of Scarab-Dd well. A drift-curve (in blue middle track) is defined as a measure of the difference between the two time-depth relationships, shown on the left-hand side. On the right panel, the black track is the original sonic log and the red track is the theoretically corrected sonic log. (B) Statistical wavelet with time response on top and respective amplitude spectrum on the bottom. The phase is constant 180° for post-stack seismic data. (C) An example of the well tie of Scarab-Dd well. The blue seismic traces are the calculated synthetic and the red represents the real seismic data using statistical wavelet shown in (B).

the first classification for AVO responses that used for oil and gas identification. Fatti et al. (1994) derived and simplified Aki and Richards' approximation to derive a suitable formula for the P-wave reflection coefficient in terms of R_P and R_S.

Castagna and Smith (1994) found that the AVO product (intercept (A)*gradient (B)) can identify the low-impedance gas-sands, but it is unclear to identify and separate the gas sands with low acoustic impedance contrast from high-impedance gas sands or brine sands. Furthermore, (A+B)/2 can distinguish between gas-sands from brine-sands easily. Foster et al. (1993, 2010) described that sands can have higher or lower acoustic impedance than surrounding shale, but gas sands have a lower Poisson's ratio than shale or brine sands. Rutherford and Williams (1989) classified different amplitude responses of gas-sands surrounded by shale into three main classes. Class I represent the changes include sands with high acoustic impedance, class II represents sands surrounded by shale with near acoustic impedance and class III for low acoustic impedance sands. Class IV was added to the AVO classes by Castagna and Swan (1997). In class IV, the normal reflection coefficient is negative and decreases while offset increases (Fig. 3A). Fig. 3B shows a color scheme used to classify seismic anomalies based on Rutherford and Williams' (1989) classification. Physical properties of different lithologies and AVO responses can be identified by creating a synthetic model through tying between well-logs to seismic data. Bright spots can be considered as strong evidence to identify the gas zones (Ismail et al., 2019), but hydrocarbons are not the only reason to produce bright spots. The seismic response is affected by the physical properties of the pore fluids in a porous rock containing those fluids (Cardamone et al., 2007). Chiburis et al. (1993) described the AVO analysis using special data to identify the change in lithology from fluid changes. Reflection coefficient based on the Amplitude Versus Angle (AVA) and

Please cite this article as: Ismail, A et al., Application of AVO attributes for gas channels identification, West offshore Nile Delta, Egypt, Petroleum Research, https://doi.org/10.1016/j.ptlrs.2020.01.003

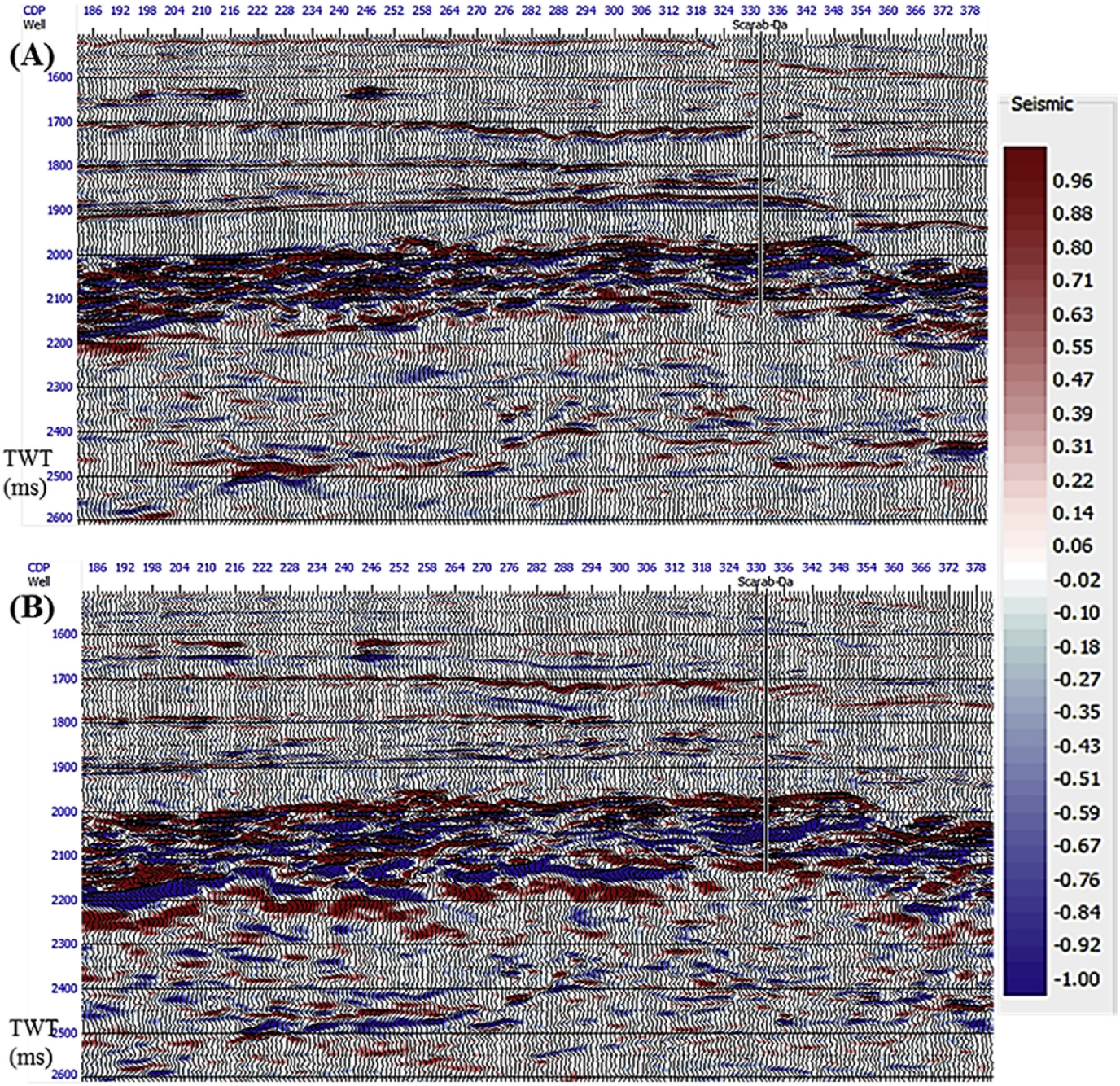

Fig. 6. (A) Extracted intercept. (B) Extracted gradient.

therefore based on Amplitude Versus Offset (AVO) too which refers to reflection dependence on the angle and offset. AVO technique represents a Direct Hydrocarbon Indicator (DHI), lithologies separation and fluid types identification using angle-stack seismic data based on the amplitude contrast in interfaces which affected by abrupt change in the physical properties.

2. Methodology

2.1. Data analysis

The data used in the study consisting of well-logs of five wells drilled in East Mediterranean, West Delta Deep Marine (WDDM), Egypt (Fig. 1). These wells are named Scarab-1, Scarab-De, Scarab-Da, Scarab-Dd, and Scarab-2, with composite logs of gamma-ray, resistivity, and Vp sonic. We have used angle-stacks seismic data with near, mid, and far offsets supported by the well-logs to perform the analysis. Fig. 4 illustrate the work flowchart starting from the data conditioning of the well logs and seismic data.

Seismic data conditioning was performed by applying trim statics and amplitude balance corrections before creating the synthetic seismogram for helping us to measure the correct amplitude variation with increasing the angle and offset. Tying well logs to the seismic data at the correct location is an essential step for the AVO analysis as it is used to identify horizons to be picked for the initial model and for estimating the wavelet. Incorrect well ties can lead to

Please cite this article as: Ismail, A et al., Application of AVO attributes for gas channels identification, West offshore Nile Delta, Egypt, Petroleum Research, https://doi.org/10.1016/j.ptlrs.2020.01.003

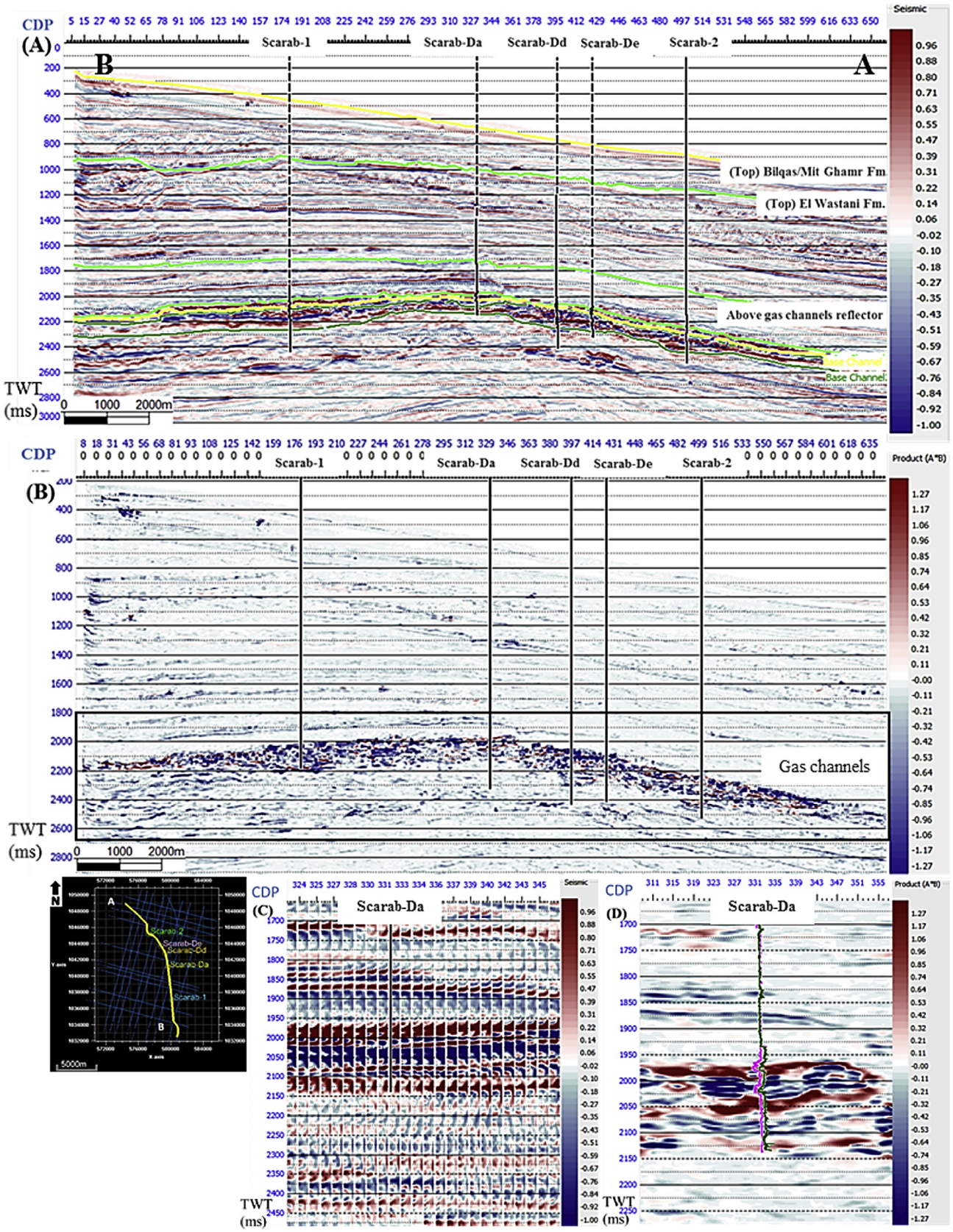

Fig. 7. (A) Original seismic gathers. (B) Show a correlation between AVO classes 1 and 3. After zooming on Scarab-Da well, (C) Original seismic gathers. (D) Show a correlation between AVO classes 1 and 3 supported by gamma ray and P-wave logs of Scarab-Da well with green and magenta colors respectively.

Please cite this article as: Ismail, A et al., Application of AVO attributes for gas channels identification, West offshore Nile Delta, Egypt, Petroleum Research, https://doi.org/10.1016/j.ptlrs.2020.01.003

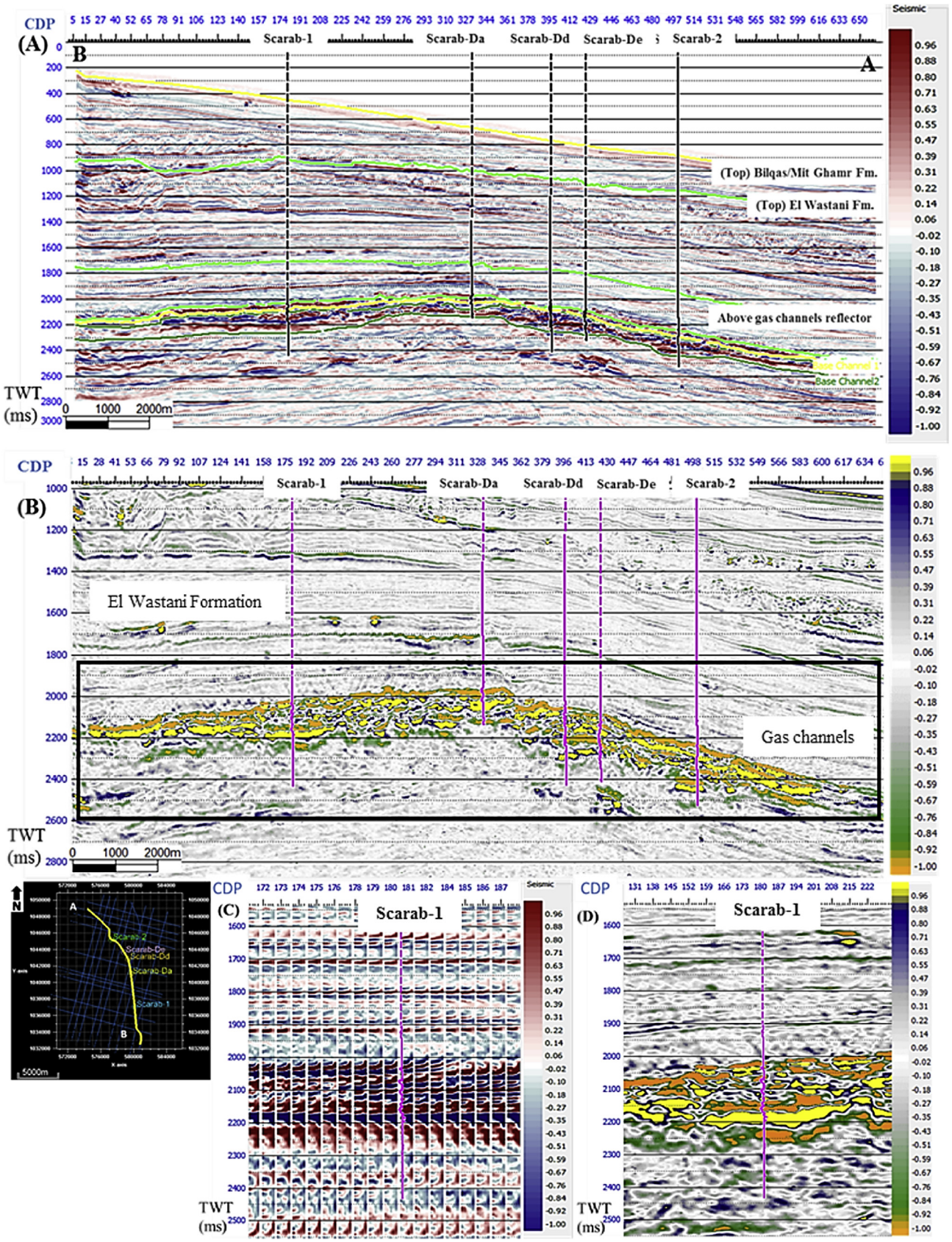

Fig. 8. (A) Original seismic gathers. (B) Scaled Poisson's ratio show variation depending on the fluid content of the reservoir where low values are a good direct indicator for gas saturated sand. After zooming on Scarab-1 well, (C) Original seismic gathers. (D) Poisson's ratio show variation due to the fluid content of the reservoir where low values are a good direct indicator for gas supported by Scarab-1 well Vp log with magenta color.

Please cite this article as: Ismail, A et al., Application of AVO attributes for gas channels identification, West offshore Nile Delta, Egypt, Petroleum Research, https://doi.org/10.1016/j.ptlrs.2020.01.003

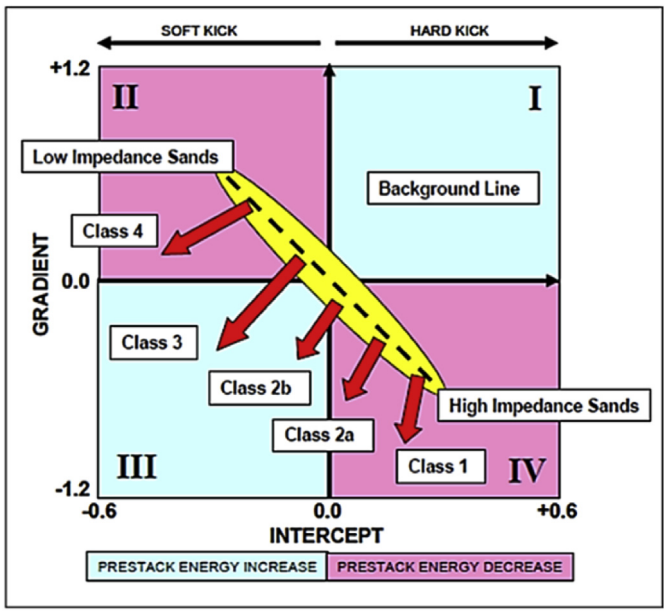

Fig. 9. Crossplot diagram (Castagna and Swan, 1997).

unreliable models upon which the inversion is based and thus reduce the confidence in the inverted volume. The first step of the well tie procedure is the calibration of the sonic log and the check-shot, by matching the time-depth relationship from the integrated sonic log to the time-depth relationship from the check-shot survey.

The wavelet that gives an optimum tie of a well log to a seismic section has a characteristic phase, frequency, and amplitude. It is common to extract the seismic wavelet using the statistical method (Nanda, 2016). This process implicates the comparison between the real seismic data with the synthetic trace (Fig. 5). If the calibration results give a good correlation with the consideration of fresnel zone parameter, then the seismic can be in terms of geology. If the calibration results are bad, there will stay major uncertainty in the interpretation of seismic data (Chopra and Sharma, 2016). The statistical wavelet extraction process uses auto-correlation and assumes a user-defined constant phase. A zero-phase assumed as the processing of the seismic would have implemented this by convolving the seismic data with an inverse filter that converts the estimated wavelet in the data to a zero-phase equivalent. With our current seismic polarity (trough is a result of the increase in acoustic impedance), the phase of the extracted wavelets will have a reverse SEG polarity (180° phase shift) (Fig. 5B). The extraction of the statistical wavelet is done in the time window with the reliable matching between seismic and synthetic reflectivity. A constant computation window of 700 ms (between 1600 ms and 2300 ms), 200 ms in length with a 25 ms taper (Fig. 5). Then, as shown in (Fig. 5C), the synthetic seismogram was created using the same parameters.

AVO analysis is started with extracting AVO common attributes including intercept (A) and gradient (B) (Fig. 6) to be able to apply A/B (Two-term Aki-Richards), A*B and A+B for Scaled Poisson ratio change and generate crossplots to identify and separate reservoir fluids and different lithological units. AVO cross plotting can be used to determine AVO class (Castagna and Swan, 1997) and identify hydrocarbon sediments (Ross and Kinmann, 1995). Under different geological conditions, intercept (A) and gradient (B) values in shale and water sand layers show a particular trend of background. AVO anomalies represent any deviation from this trend of background that may be due to lithology factors or hydrocarbon presence.

3. Results and discussion

3.1. AVO attributes

The AVO attributes can identify and distinguish between the change in lithology and fluid content by the anomalies that we can get from the AVO analysis.

3.1.1. Intercept product gradient (A*B)

The calculation of intercept (A) and gradient (B) from the pre-stack seismic dataset proceeds using the velocity data from well logs. The result from the (A*B) is always positive (red color) in the AVO class III, because the sign of both the gradient and the intercept are the same (positive or negative), while in class I, they have different signs (positive and negative), so the product is always negative (blue color) in Fig. 7.

Fig. 7 illustrates the AVO response derived from the product of the intercept and gradient (A*B). In this figure, the color display represents the product of the intercept and gradient which highlights the AVO anomaly. By calibration of this AVO anomaly with resistivity, Vp, and gamma ray logs, we find that there is compatibility between the gas saturated sand and the AVO response.

3.1.2. Poisson's ratio change

Poisson's ratio is one of the best indicators for the presence of gas saturated sediments. Scaled Poisson's ratio AVO attribute shows variation based on the fluid content of the reservoir. The extraction of this attribute is considered the best way to show the AVO anomaly using the color data show the scaled Poisson's ratio values at the two-way time between 1900 and 2500 ms (Fig. 8B). By calibration of the change in Poisson's ratio with resistivity, Vp, and gamma ray logs, we find that there is compatibility between the gas saturated sand and the low scaled Poisson's ratio values (Fig. 8D). The recognition that hydrocarbons affect the acoustic impedance and Poisson's ratio of sandstones reservoir lead to the development of seismic attributes to detect these effects.

The AVO sum (A+B) shows a negative response at the top of the reservoir (a decrease in Poisson's ratio) and a positive response at the base (an increase in Poisson's ratio), indicating hydrocarbon-charged sands. This attribute works well for Class 2 and 3 AVO responses (Ross, 2002).

3.2. AVO crossplots

Castagna and Swan (1997) pointed out that the cross-plotting technique is the easiest method to derive relationships between different variables. We use this technique to plot the AVO intercept attribute (A) on the X-axis and AVO gradient (B) on the Y-axis, the I and III sectors of the diagram, Fig. 9 thus represent the pre-stack energy increase domain (positive AVO restricted gradient); II and IV sectors represent the pre-stack energy decrease domains (negative AVO restricted gradient); the left half of the diagram corresponds to soft kicks and the right to hard.

Basic theory places normal AVO of sediments (shale and wet sands) within the pre-stack energy decrease domains (pink quadrants), the variability of sediment petro-acoustic characteristics distributes the intercept-gradient pairs along a line passing through the origin and crossing the II and IV quadrants, it is called the background line and its dip depends both on the depth of burial considered and on the specific Vp/Vs ratio (Castagna's mudrock line) in Fig. 9. If hydrocarbon is introduced in high impedance sands, intercept slightly decreases and negative gradient strongly

Please cite this article as: Ismail, A et al., Application of AVO attributes for gas channels identification, West offshore Nile Delta, Egypt, Petroleum Research, https://doi.org/10.1016/j.ptlrs.2020.01.003

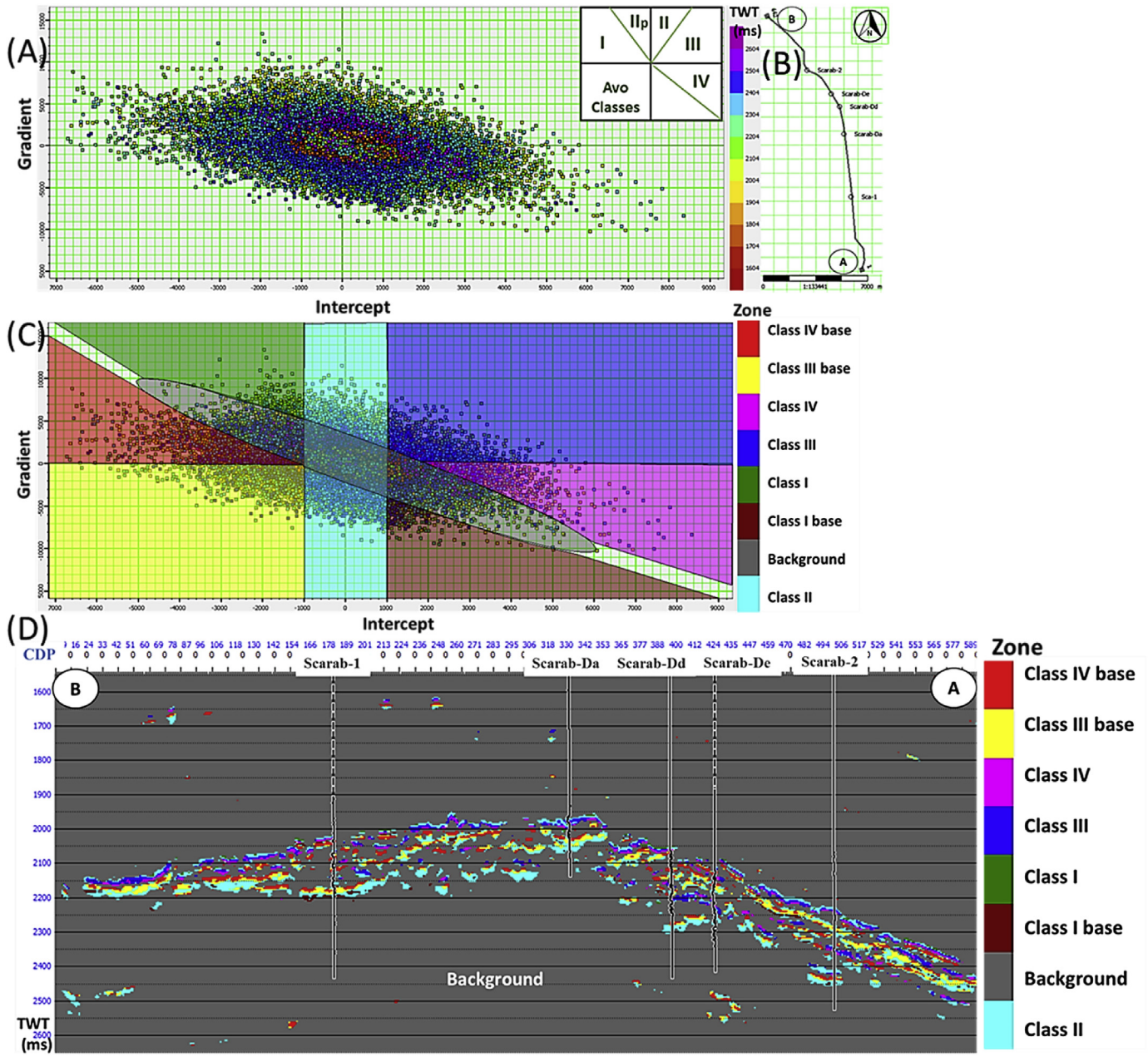

Fig. 10. (A) AVO intercept (A) and gradient (B). (B) Location of the arbitrary line. (C) After identifying the classes for each AVO anomaly zone in (A) with different colors. (D) A seismic cross section highlighting AVO anomalies with the Vp log (in black).

increases its absolute value, the result is a deviation from the background line within the IV quadrant (class 1 anomaly). When hydrocarbons are introduced in sands having impedance close to the sealing limit, the intercept moves toward more negative values and sign change may even occur. The gradient moves to high negative resulting in a cluster positioned within the III quadrant and partially invading the IV one (class 2). Finally, if hydrocarbons are introduced to low impedance sands, the intercept becomes more negative and the gradient approaches zero, the resulting cluster appears far away from mudrock line and centers on the X-axis, covering both the III (class 3) and II quadrants (class 4) (Castagna and Swan, 1997). A more practical approach, that has been done, is to crossplot the intercept and gradient for all the time samples at all the trace locations within a specific window. Deviation from this regime may be a hydrocarbon indicator. The intercept and gradient pairs move more away from the background trend, with a decrease in the fluid density, so that gas sands will be the most well-separated (Fig. 10).

The degree of the shift away from the background trend (AVO anomalies) is due to the stiffness of the rock, its fluid content, and its porosity. AVO analysis and interpretation is done by defining the background trend and defines the points moved far away from the background trend, which are highlighted with several colors due to its AVO class to indicate the top and base-gas zones in the crossplot (Fig. 10C) before projecting these anomalies to the seismic section with its corresponding TWT and offset or angle (Fig. 10D).

The classification of AVO responses should be based on the position of the reflection of interest on an A versus B cross-plot (Fig. 11). Class I sand is generally found in a hard-rock and has a higher impedance than the encasing shale material and the polarity

Please cite this article as: Ismail, A et al., Application of AVO attributes for gas channels identification, West offshore Nile Delta, Egypt, Petroleum Research, https://doi.org/10.1016/j.ptlrs.2020.01.003

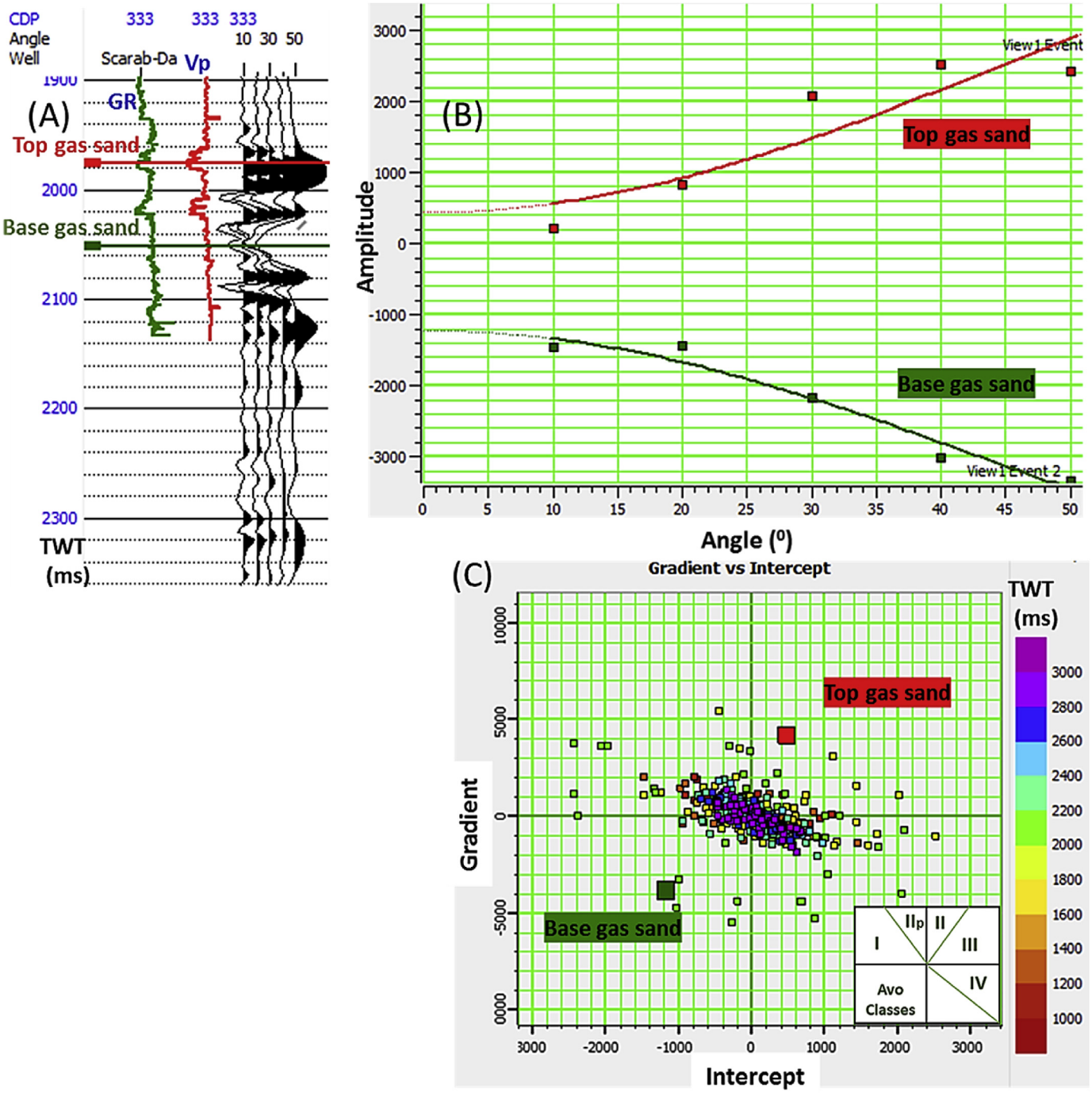

Fig. 11. (A) The theoretical AVO model on seismic traces at Scarab-Da well location, (B) amplitude-angle crossplot and (C) intercept-gradient crossplot and the scheme shows the AVO classification.

changes associated with them that produce dim out effects in stacked seismic data. Class II sands are found in onshore and offshore exploration areas. They have almost the same impedance as the encasing shale. Class II sands can have dramatic AVO effects if an adequate angle/offset range is available in the seismic data. The stacked response of Class II sands, such as the Miocene age gas-sand. Class III sands are found mainly in marine environments and have lower impedance than the encasing shale. Plio-Pleistocene gas sands are usually Class III sands (Rutherford and Williams, 1989). Class IV is low impedance gas sand for which reflection coefficient decrease with increasing offset; that may occur, for example, when the shear-wave velocity in the gas sand is lower than in the overlying shale (Castagna and Swan, 1997).

AVO response over both gas sands and wet sands that is much closer to theoretically expected values. As shown in Figs. 11 and 12, using the Scarab-Da and Scarab-Dd wells supported by well logs as examples, the AVO synthetic model shows a typical class II response for top and base gas sand in Fig. 11 using Scarab-Da well while it shows a typical class IV response for top and base gas sand in Fig. 12 using Scarab-Dd well.

Please cite this article as: Ismail, A et al., Application of AVO attributes for gas channels identification, West offshore Nile Delta, Egypt, Petroleum Research, https://doi.org/10.1016/j.ptlrs.2020.01.003

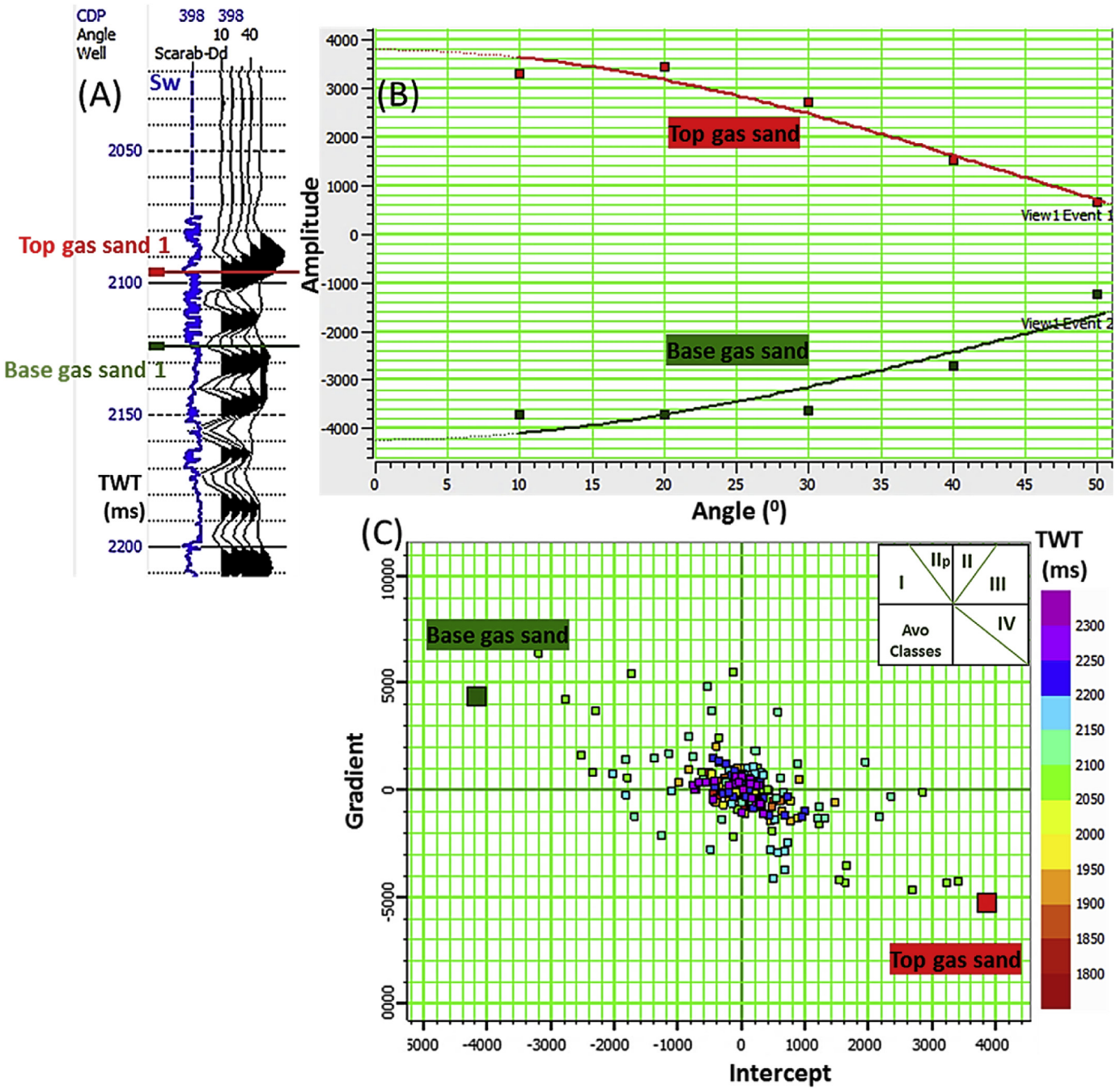

Fig. 12. (A) The theoretical AVO model on seismic traces at Scarab-Dd well location, (B) amplitude-angle crossplot and (C) intercept-gradient crossplot and the scheme shows the AVO classification.

4. Conclusion

The main aim of work, identification of the gas-sand zones in the Late Pliocene El-Wastani formation. AVO attributes (also called indicators) are used and crossplots are generated. As we move beyond simple anomaly hunting, AVO provides an important fundamental understanding of seismic amplitudes. The product indicator (A × B) works well with classes I and III sands (Fig. 7), and it has the advantage of inheriting some of the lateral coherency of the intercept which can be a significant aid in interpretation. Scaled Poisson's ratio attribute is evaluated to determine the gas channels through the seismic section in Fig. 8 and the fluid changing boundary can be specified clearly. Poisson's ratio shows variation due to the fluid content of the reservoir where low values are a good direct indicator for gas zones.

The AVO analysis shows that the gas channels in El Wastani Formation belong to classes I, II, III, and IV as shown in the seismic cross-section highlighting AVO anomalies in Fig. 10. Using this color scheme, four zones of AVO response were outlined on the AB crossplot shown in Fig. 10C. These responses are mapped back to the seismic section where they carefully picked out the top and bottom reflectors from the gas sands (Fig. 10D). Two crossplot examples are presented as shown in Figs. 11 and 12, using the scarab-Da and scarab-Dd wells supported by well logs, the AVO synthetic model

Please cite this article as: Ismail, A et al., Application of AVO attributes for gas channels identification, West offshore Nile Delta, Egypt, Petroleum Research, https://doi.org/10.1016/j.ptlrs.2020.01.003

shows a typical class II response for top and base gas sand in Fig. 11 using Scarab-Da well and shows a typical class IV in Fig. 12 using Scarab-Dd well for specified TWT window.

Acknowledgements

The authors would gratefully express their appreciation to Egyptian General Petroleum Corporation (EGPC), Rashid Petroleum Company (Rashpetco) for providing the data needed to perform this work and giving permission to publish this work, and to the Egyptian cultural affairs and missions sector to give the opportunity to Mr. Amir Ismail to finish this work at Seismological Laboratory (RISSC-Lab), Department of Physics E. Pancini, University of Naples "Federico II", Napoli, Italy.

References

Abdel Halim, M., 2001. Future hydrocarbon potential in the Nile Delta offshore and onshore. In: Zaghloul, Z.M., El-Gamal, M. (Eds.), Deltas Modern and Ancient. Proc. 1st International Symposium on the Deltas. March 13-19, 1999, Cairo, Egypt, pp. 159e174.

Aki, K., Richards, P.G., 1980. Quantitative Seismology: Theory and Methods. W.H. Freeman and Co., San Francisco, Calif.

Cardamone, M., Ciurlo, B., Noli, V., 2007. AVO and Fluid Inversion. ENI.

Castagna, J.P., Smith, S.W., 1994. Comparison of AVO indicators: a modeling study. Geophysics 59, 1849–1855.

Castagna, J.P., Swan, H.W., 1997. Principles of AVO crossplotting. Lead. Edge 16, 337–342.

Castagna, J.P., Swan, H.W., Foster, D.J., 1998. Framework for AVO gradient and intercept interpretation. Geophysics 63 (3), 948–956.

Chiburis, E., Franck, C., Leaney, S., McHugo, S., Skidmore, C., 1993. Hydrocarbon detection with AVO. Oilfield Rev. 6, 42–50.

Chopra, S., Sharma, R.K., 2016. Preconditioning of seismic data prior to impedance inversion. Recorder 41 (3), 32–34.

Domenico, S.N., 1977. Elastic properties of unconsolidated porous sand reservoirs. Geophysics 42, 1339–1368.

Egyptian General Petroleum Corporation (EGPC), 1994. Nile Delta and North Sinai: Field Discoveries and Hydrocarbon Potentials (A Comprehensive Overview). Egyptian General Petroleum Corporation, Cairo, p. 387.

Fatti, J.L., Smith, G.C., Vail, P.J., Strauss, P.J., Levitt, P.R., 1994. Detection of gas in sandstone reservoirs using AVO analysis: a3-D seismic history using the Geostack technique. Geophysics 59, 1362–1376.

Foster, D.J., Smith, S.W., Dey-Sarkar, S., Swan, H.W., 1993. A closer look at hydrocarbon indicators. SEG Tech. Progr. Expand. Abstr. (1), 1396.

Foster, D.J., Keys, R.G., Lane, F.D., 2010. Interpretation of AVO anomalies. J. Geophys. 75, 3–13.

Ismail, A., Ewida, H.F., Al-Ibiary, M.G., Gammaldi, S., Zollo, A., 2019. Identification of Gas Zones and Chimneys Using Seismic Attributes Analysis at the Scarab Field, Offshore, Nile Delta, Egypt, Petroleum Research. https://doi.org/10.1016/j.ptlrs.2019.09.002.

Kamel, H., Eita, T., Sarhan, M., 1998. Nile delta hydrocarbon potentiality, Egypt. In: Proceedings of the 14th EGPC Exploration and Production Conference, pp. 485–503. Cairo.

Muskat, M., Meres, M.W., 1940. Reflection and transmission coefficients for plane waves in elastic media. Geophysics 5, 115–148.

Nanda, N., 2016. Seismic Data Interpretation and Evaluation for Hydrocarbon Exploration and Production. Springer, Berlin.

Nini, C., Checchi, F.E., Blasy, A., Talaat, A., 2010. Depositional Evolution of the Plio-Pleistocene Succession as a Key for Unraveling the Exploration Potential of the Post-musician Play in the Central Nile Delta. Mediterranean Offshore Conference & Exhibition, Alexandria, Egypt.

Ostrander, W.J., 1984. Plane-wave reflection coefficients for gas sands at nonnormal angles of incidence. Geophysics 49, 1637–1648.

Ross, C.P., Kinmann, D.L., 1995. Non-bright spot AVO: two examples. J. Geophys. 60, 1398–1408.

Ross, C.P., 2002. Comparison of popular AVO attributes, AVO inversion, and calibrated AVO predictions. Lead. Edge 21, 244–252.

Rutherford, S.R., Williams, R.H., 1989. Amplitude-versus-offset variations in gas sands. Geophysics 54, 680–688.

Vandré, C., Cramer, B., Gerling, P., Winsemann, J., 2007. Natural gas formation in the western Nile delta (Eastern Mediterranean): thermogenic versus microbial. Org. Geochem. 38 (4), 523–539.

Younis, A., El-Qady, G., Alla, M.A., Zaher, M.A., Khalil, A., Al Ibiary, M., Saraev, A., 2015. AMT and CSAMT methods for hydrocarbon exploration at Nile Delta, Egypt. Arabian J. Geosci. 8 (4), 1965–1975.

Please cite this article as: Ismail, A et al., Application of AVO attributes for gas channels identification, West offshore Nile Delta, Egypt, Petroleum Research, https://doi.org/10.1016/j.ptlrs.2020.01.003